

NOAA Technical Report ERL 393-SEL 40



# **The Ion-Electron Magnetic Separation and Solid State Detector Detection System Flown on IMP 7 and 8: $E_p \geq 50$ keV, $E_e \geq 30$ keV**

D. J. Williams

October 1977



U.S. DEPARTMENT OF COMMERCE  
National Oceanic and Atmospheric Administration  
Environmental Research Laboratories





**The Ion-Electron Magnetic Separation  
and Solid State Detector Detection  
System Flown on IMP 7 and 8:  
 $E_p \geq 50$  keV,  $E_e \geq 30$  keV**

D. J. Williams

Space Environment Laboratory  
Boulder, Colorado

October 1977

U.S. DEPARTMENT OF COMMERCE  
Juanita M. Kreps, Secretary

National Oceanic and Atmospheric Administration  
Richard A. Frank, Administrator

Environmental Research Laboratories  
Wilmot Hess, Director  
Boulder, Colorado



Digitized by the Internet Archive  
in 2013

<http://archive.org/details/ionelectronmagne00will>

## CONTENTS

	Page
ABSTRACT	1
1. INTRODUCTION	1
2. ENERGETIC PARTICLES EXPERIMENT	2
3. SENSOR HEADS AND ELECTRONICS	2
4. CALIBRATIONS	7
5. IN-FLIGHT PERFORMANCE	10
6. GROUND DATA HANDLING	12
7. ACKNOWLEDGMENTS	17
8. REFERENCES	17



THE ION-ELECTRON MAGNETIC SEPARATION AND SOLID STATE DETECTOR  
DETECTION SYSTEM FLOWN ON IMP 7 AND 8:  $E_p \geq 50$  keV,  $E_e \geq 30$  keV

D. J. Williams

Abstract. The Energetic Particles Experiment (EPE) carried aboard the NASA IMP 7 and 8 satellites was one of the first low energy (tens of kilovolts) magnetic/solid state detector ion-electron separation and analysis systems flown in space. Although we are now constructing substantially more sophisticated systems for space flight, it remains of interest to describe this early instrument, its calibration, its in-flight operation, and its ground data handling and display system. Normal operation with no failures has gone on for a combined IMP 7 and 8 total of 8.5 years in orbit.

## 1. INTRODUCTION

This paper describes an ion-electron solid state detector/magnetic deflection system flown aboard the NASA satellites IMP 7 (Explorer 47) and IMP 8 (Explorer 50). This instrument represents our initial effort in a series of such instruments whose goal is to achieve clean ion-electron separation down to energies of a few tens of keV at low weight and relatively large geometric factors. This goal has been achieved, and follow-on instrumentation has been flown on board the earth orbiting satellites Explorer 45 (Williams et al., 1969; Longanecker and Hoffman, 1973) and ATS-6 (Fritz and Cessna, 1975) and the solar orbiting satellites Helios 1 and 2 (Keppler et al., 1976). Significantly improved instrumentation has been fabricated for the ISEE A and B spacecraft and will be described in a future paper.

The IMP 7 and 8 energetic particle experiment (EPE) cleanly separates ions and electrons in the energy range from 30 keV through several MeV. In addition to the magnetic deflection system, complementary particle observations are obtained from a low-noise detector ( $\sim 18$  keV discriminator level) and a thin ( $\sim 5 \mu$ ) detector.

IMP 7 and 8 were launched on September 23, 1972, and October 28, 1973, respectively, into roughly circular orbits (in the solar ecliptic plane) at a geocentric distance of  $\sim 35$  Earth radii ( $35 R_E$  224,000 km). Both satellites were spin stabilized (IMP 7, 48 RPM; IMP 8, 24 RPM) with their spin axes oriented perpendicular to the ecliptic plane. IMP 8 was initially positioned  $\sim 180^\circ$  from IMP 7. Subsequent in-orbit drift decreased the satellite separation distance until a minimum separation of  $\sim 2.5 R_E$  was reached on

February 2, 1976, after which the separation distance once again slowly increased. These orbits have allowed a variety of solar-terrestrial studies using simultaneous observations from nearly identical instruments over a wide range of spatial separations in the Earth's magnetotail and magnetosheath, and in near-Earth interplanetary space.

The EPE's on both IMP 7 and 8 have functioned normally up to the present with no malfunctions or failures. The following sections describe the instrument, its in-flight operation, and samples of ground data displays.

## 2. ENERGETIC PARTICLES EXPERIMENT (EPE)

The EPE instrument is shown in Figure 1 in a standard IMP package configuration. Package depth and height are 25.4 cm and 12.7 cm, respectively. The EPE weighs 3.18 kg and requires a normal power of 2.6 watts. Power levels during command and calibrate sequences are 2.8 and 3.1 watts, respectively. One full 15° viewing cone perpendicular to the spin axis and two full 13° viewing cones 45° to the spin axis are used for the EPE particle observations. Angular distributions are measured by obtaining 8 or 16 samples (depending on particle type and energy) per satellite spin period. The effective bit rate of the EPE is ~18.8 bits per second and a complete energy-angular distribution sample is obtained every 20.4 seconds.

Comprehensive analog and digital housekeeping systems are used to keep track of experiment status and operational condition. For example, routine measurements are made of all detector-preamplifier RMS noise levels for comparison with prelaunch values. An extensive command system



Figure 1. Assembled EPE package.

is used to control power supplies, discriminator levels, and logic selections. An electronic in-flight calibrator (Peletier, 1970) provides a thorough check of experiment electronics from the preamplifiers through the output logic and permits routine calculations of discriminator level settings for comparison with prelaunch calibrations.

These in-flight tests have shown the IMP 7 and 8 EPE's to have operated in a completely normal fashion to the present time, a total of ~8.5 years of in-flight operation.

## 3. SENSOR HEADS AND ELECTRONICS

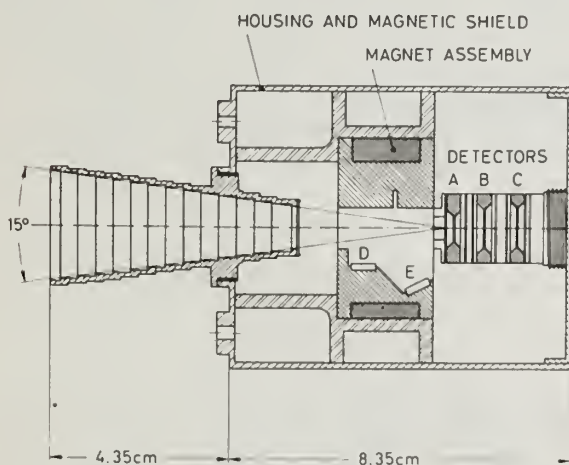
The EPE particle detector assembly consists of a main magnet-detector assembly and two auxiliary detector heads. All detectors are fully depleted, surface barrier, solid state detectors, and are operated with bias voltages 1.25-1.5 times the values required for full depletion. To minimize radiation damage effects, all detectors directly exposed to ion fluxes are mounted with the aluminum contact exposed to the incoming beam. In this way catastrophic detector failure due to radiation damage is

extended to the  $10^{16}$ - $10^{18}$  protons/cm<sup>2</sup> range (Coleman et al., 1968 a,b). On the basis of observed fluxes, radiation damage is not yet a problem for the EPE.

The main magnet-detector assembly is shown schematically and in various stages of completeness in Figure 2. It consists of a three-element telescope (detectors A, B, C), a sweeping magnet that keeps low energy electrons ( $E_e \lesssim 200$ -300 keV) away from the telescope, and two detectors (D and E) to detect the

swept electrons. The telescope covers the proton energy range 50 keV  $\leq E_p \leq 25$  MeV and the alpha particle energy range 2.2 MeV  $\leq E_\alpha \leq 35$  MeV. Detectors D and E cover the electron energy range 30 keV  $\leq E_e \leq 200$  keV. The magnet has a peak strength of  $\sim 1000$  Gauss. A high permeability nickel-iron-magnesium alloy can enclose the entire assembly, keeping the stray magnetic field from the EPE at  $\lesssim 0.15$  nT (1 nT =  $10^{-5}$  Gauss) at 2 meters and thus satisfying the IMP 7 and 8 magnetic cleanliness requirement.

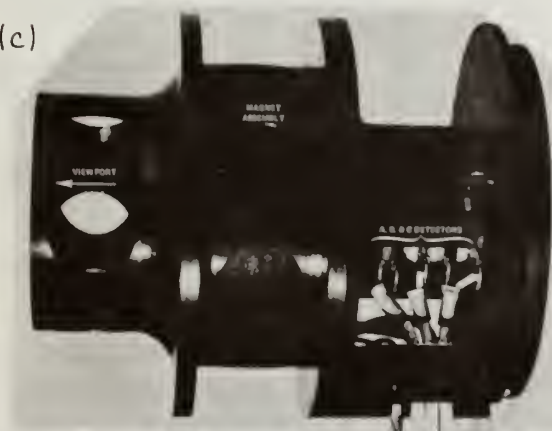
(a)



(b)



(c)



(d)



Figure 2. Main magnet assembly of EPE. (a) Schematic showing detector, magnet, structure, and housing, (b) Photograph of detector assembly showing all detectors, (c) Photograph showing assembled internal structure without magnet assembly, (d) Fully assembled magnetic configuration showing shielding can and collimator. Look-angle is oriented 90° to satellite spin axis.

The housing for the auxiliary detectors (F and G) is shown schematically in Figure 3. Detector F is a selected low-noise device employing a single discriminator in the 15-20 keV region to measure low energy protons and electrons. Detector G is a very thin ( $\sim 5 \mu$ ) device employing discriminator levels to measure alpha particle and  $Z \geq 3$  particle intensities. The characteristics of the IMP 7 and 8 EPE detectors G have been described in detail by Wilken and Fritz (1974, 1976; their detectors D8 and D5).

The detector ABC telescope has the following geometric factors: detector A,  $1.11(10)^{-2} \text{cm}^2 \text{ster}$ ; detector AB,  $1.07(10)^{-2} \text{cm}^2 \text{ster}$ ; detectors ABC,  $0.97(10)^{-2} \text{cm}^2 \text{ster}$ . The electron detectors, D and E, have a maximum calculated geometric factor of  $0.97(10)^{-2} \text{cm}^2 \text{ster}$ . Accounting for measured energy and angle-dependent efficiencies, approximate detector D and E geometric factors are  $1.5(10)^{-3} \text{cm}^2 \text{ster}$  and  $0.9(10)^{-3} \text{cm}^2 \text{ster}$ . Detector characteristics, discriminator levels, and logic outputs are given in Tables 1 and 2. A simplified block diagram is shown in Figure 4.

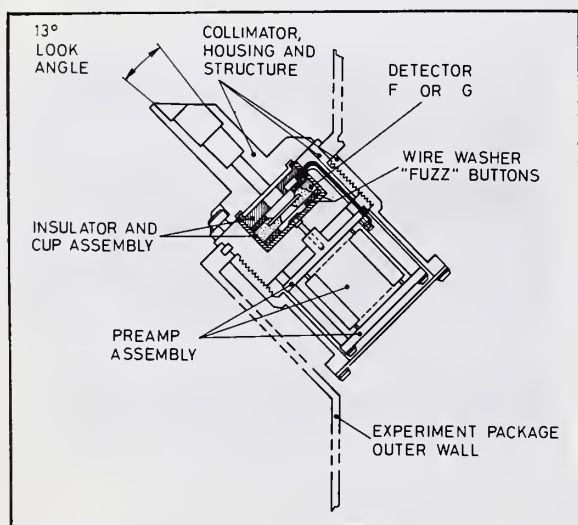


Figure 3. Schematic showing housing for detectors F and G. Look angle oriented  $45^\circ$  to satellite spin.

TABLE 1. EPE DETECTOR CHARACTERISTICS

Detector	Area* (mm <sup>2</sup> )	Thickness ( $\mu$ )	Bias Voltage	Current ( $\mu$ A)
<u>Satellite 7</u>				
A	25	54.2	30	.25
B	50	514	150	.55
C	50	501	150	.66
D	18	300	150	.27
E	18	300	150	.32
F	25	100	30	.08
G	10	6.0	2.5	.007
<u>Satellite 8</u>				
A	25	54.7	30	.23
B	50	491	150	.27
C	50	508	150	.52
D	18	300	150	.54
E	18	300	150	.30
F	25	100	30	.09
G	10	5.87	1.6	.03

\*Detectors D and E are 6mm x 3mm rectangular units. All others are circular.

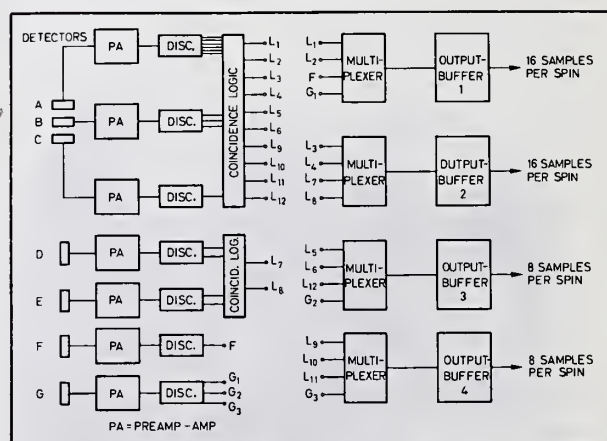


Figure 4. Simplified block diagram of EPE electronics. Calibration, housekeeping, command, and timing functions are not shown. In case of logic failure, discriminator level output can be routed by command to the multiplexers.

TABLE 2. EPE NORMAL DISCRIMINATOR LEVELS AND OUTPUT LOGIC

Detector	Discriminator* Levels (MeV)		Logic	Output Channels (MeV)	Designation	Nuclear Charge Range	Samples per spin
A	A1	0.03	$A_1 \bar{A}_2 \bar{B}_1$	0.05 - 0.22	$L_1$	$Z \geq 1$	16
	A2	0.20	$A_2 \bar{A}_4 \bar{B}_1$	0.22 - 0.80	$L_2$	$Z \geq 1$	16
	A3	0.50	$A_3 \bar{A}_4 B_2 \bar{B}_3 C$	4.5 - 8.5	$L_5$	$Z = 1$	8
	A4	0.80	$A_4 \bar{A}_5 \bar{B}_1$	0.80 - 2.1	$L_3$	$Z \geq 1$	16
	A5	2.5	$A_4 \bar{A}_5 B_1 \bar{B}_2 C$	2.1 - 4.5	$L_4$	$Z = 1$	16
	A6	3.5	$A_6 B_1 \bar{C}$	8.4 - 16.0	$L_{11}$	$Z = 2$	8
B			$\bar{A}_2 B_1 \bar{C}$	background	$L_9$		8
	B1	0.10	$A_5 \bar{B}_1$	2.2 - 8.4	$L_{10}$	$Z \geq 2$	8
	B2	3.6	$A_5 \bar{A}_6 B_2 \bar{C}$	16.0 - 35.0	$L_{12}$	$Z = 2$	8
	B3	9.0					
C	C	0.10	$A_2 B_1 C$	8.5 - 25.0	$L_6$	$Z = 1$	8
D	D1	0.030	$D_1 \bar{D}_2$	0.03 - 0.10	$L_7$	electrons	16
	D2	0.100					
E	E1	0.100	$E_1 \bar{E}_2$	0.10 - 0.20	$L_8$	electrons	16
	E2	0.200					
F	F1	0.015	$F_1$	>0.015	F	electrons and ions	16
G	G1	0.60	$G_1$	>0.6	$G_1$	$Z \geq 2$	16
	G2	1.0	$G_2$	>1.0	$G_2$	$Z \geq 2$	8
	G3	2.0	$G_3$	>2.0	$G_3$	$Z \geq 3$	8

\* Levels  $A_1$  and  $D_1$  are commandable to 50 keV. Level  $F_1$  is commandable to 30 keV.

\*\*Low energy proton response is 50 keV due to aluminum dead layer.

For the same reason, detector F low energy proton response is 0.024 MeV and 0.038 MeV on IMP 7 and 8 respectively.

As a safeguard against possible failure in the logic circuitry, a commandable mode was incorporated into the EPE whereby all discriminator levels could be routed to the multiplexers, thereby giving discriminator output counts only. Further safeguards include commandable low-level discriminators on detectors A, D, and F to protect against possible

detector noise increases, and bias voltages commandable in four steps from normal operating bias to one-half that value to guard against excessive detector bias current. None of these safeguard modes has been required to date. For reference, routinely monitored EPE status and housekeeping functions are listed in Tables 3 and 4.

TABLE 3. EPE STATUS MONITORS

EPE Status Indicator	Function
1	Calibrator ON/OFF
2	A <sub>1</sub> Level 30/50
3	D <sub>1</sub> Level 30/50
4	F Level 15/30
5	Spare
6	30 V Supply. Level set at
7	30, 27, 24, or 15 V
8	Detector C Coincidence ON/OFF
9	150 V Supply. Level set at
10	150, 135, 120, or 75 V
11	Command System GO/NO GO
12	Calibrator Power ON/OFF
13	Timing Information
14	Test Connector Activated/Not Activated
15	Spare
16	Logic or Discriminator Output

TABLE 4. EPE HOUSEKEEPING MEASUREMENTS

EPE Analog Measurement	Function
1	Temperature
2	150 V Bias Line
3	Variable 150 V Line
4	Variable 30 V Line
5	20 V Buss
6	Reference Ground
7	5 V Reference
8	6 V Buss
9	-6 V Buss
10	A Channel Noise
11	B Channel Noise
12	C Channel Noise
13	D Channel Noise
14	E Channel Noise
15	F Channel Noise
16	G Channel Noise

Each EPE preamplifier (Gary, 1970; Hogrefe, 1970) is a common source FET stage driving a PNP common base with an NPN emitter follower. A preamplifier circuit is shown in Figure 5 for the low energy A, D, and F detectors. The emitter follower base resistor and the stray capacitances from the base interconnection are "boot-strapped" to obtain high gain and bandwidth. The use of the guard ring around the interconnection between the PNP and NPN almost doubles the band width of the circuit. All EPE preamplifiers have a test input accessible externally for last-minute calibration checks in the spacecraft.

As the EPE uses no foils in front of the detectors, the preamplifier design had to accommodate the existence of a sun pulse on detector A once each spin (e.g., a 78-millisecond sun pulse illuminates the aluminum contact of detector A during each spin of IMP 7). Several months of prelaunch laboratory tests showed

that such solar stimulations do no apparent harm to the detector. However, to insure rapid preamplifier recovery and to avoid breakdown of the FET gate-to-source junction in reverse bias, a 0.001  $\mu$ F input coupling capacitor, 10 M $\Omega$  bias and feedback resistors ( $R_b$  and  $R_{fb}$ ), and protective diodes were employed. Tests showed the 2N2369 to be suitable for use in the low-noise channels and the 1N3064 to be suitable in the less stringent noise channels. The resulting preamplifier noise

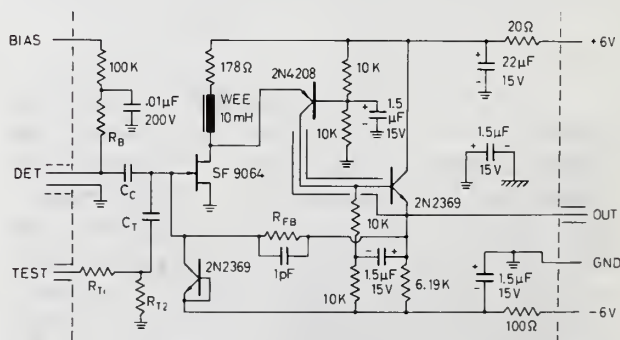


Figure 5. Schematic of detector A preamplifier.

curve is shown in Figure 6. No deleterious effects have been observed in detector A in-orbit operation. Because of the relatively thick (0.054 and 0.060 mg/cm<sup>2</sup>) aluminum layer, detector A shows no response to the sun stimulus. However, detector D sees light reflected from detector A, and data loss occurs for the solar oriented sector and four succeeding sectors.

#### 4. CALIBRATIONS

Calibrations of the EPE were performed at the Goddard Space Flight Center and Naval Research Laboratory accelerator facilities. An example of the high energy calibrations ( $E_p \lesssim 1$  MeV) performed at the Naval Research Laboratory is given in Figure 7, where we show absolute efficiencies for the L3 and L11 levels in the IMP 7 EPE. These results agree well with the normal passband values given in Table 2.

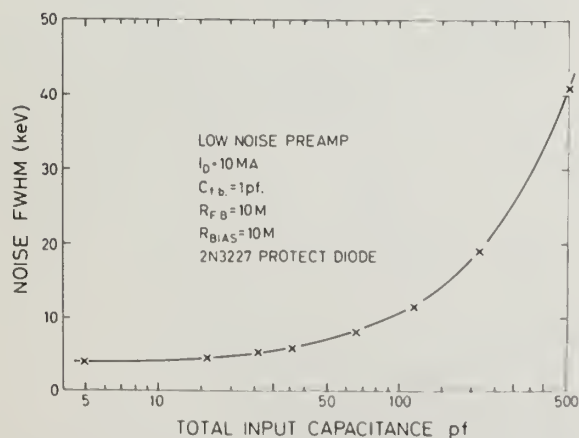


Figure 6. Noise versus input capacitance for detector A preamplifier with protection diode and 10 M $\Omega$  feedback and bias resistors.

Since protons and electrons in the low tens of keV range were being separated and measured for the first time in interplanetary space by using surface barrier solid state detectors, considerable attention was given to the low energy calibrations, all performed at Goddard Space Flight Center. Figure 8 shows the absolute detection efficiency for the lowest level of EPE detector A. Both IMP 7 and 8 results are shown for an A<sub>1</sub> discriminator level of 30 keV. The resulting 50% efficiency points of 50 keV and 52 keV for IMP 7 and 8 give respective aluminum layers of 54  $\mu$ g/cm<sup>2</sup> and 60  $\mu$ g/cm<sup>2</sup>. These are to be considered effective aluminum layers as they include the effects of any silicon dead layer and pulse height defects. Although we were unable to obtain thinner aluminum layers for the IMP 7 and 8 EPE units, we have since purchased and flown a number of detectors with significantly thinner ( $\sim 20$ -40  $\mu$ g/cm<sup>2</sup>) aluminum layers. In addition, P-type surface barrier detectors have been produced having thin ( $\sim 10$   $\mu$ g/cm<sup>2</sup>) palladium windows (Elad et al., 1973; Inskeep et al., 1974).

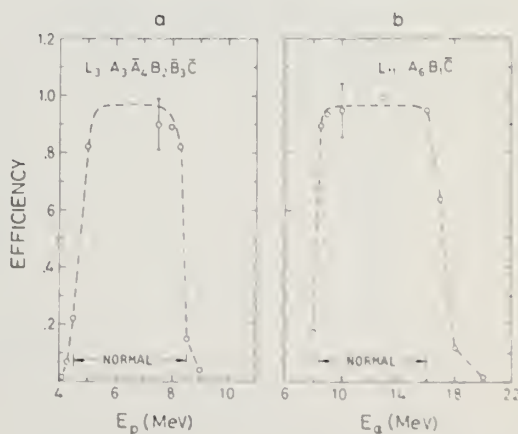


Figure 7. Absolute efficiency of EPE L<sub>3</sub> and L<sub>11</sub> logic levels obtained from accelerator calibration. Normal bandwidth from Table 2 shown for comparison.

The IMP-8 EPE  $\Delta E$  versus  $E$  curves for the ABC telescope are shown in Figure 9. The ideal detector A curve is shown as a dashed line and the actual curve, including the  $60 \mu\text{g}/\text{cm}^2$  aluminum layer, is shown as the solid line.

A calibration run was performed to measure the effectiveness of the sweeping magnet to keep low energy electrons from detector A. In addition, runs were performed at higher energies to measure the effectiveness of the coincidence circuitry and to measure effects of large-angle electron scattering in detector A. These results are shown in Figure 10 where the absolute electron detection efficiency in detector A is plotted against electron energy. It can be seen that electron-ion separation is very clean over our energy range.

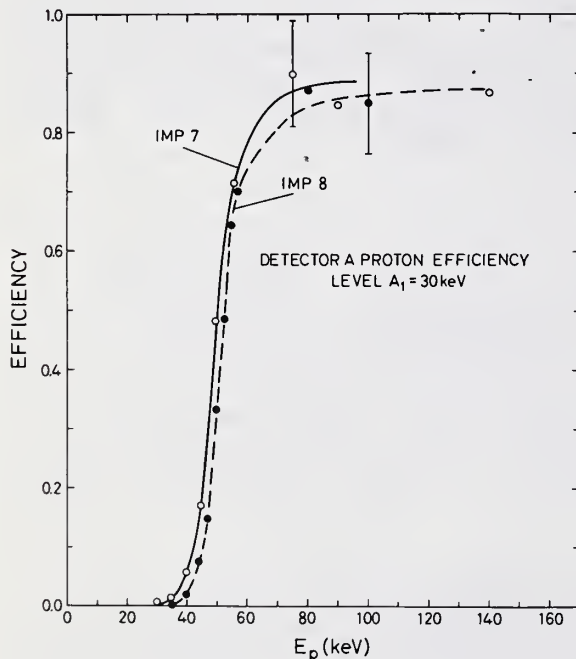


Figure 8. EPE low energy proton detection efficiency for main magnet assembly. Error bars of  $\pm 10\%$  are estimated for the absolute efficiency normalizations.

Note that while a few electron energies in the 130 keV range attain a  $3-4(10)^{-3}$  probability of reaching detector A, this probability is generally  $<10^{-3}$  and is  $<10^{-4}$  for  $E_e < 50$  keV.

Detector F proton and electron efficiencies are shown in Figure 11. Comparing the F discriminator level setting with the proton 50% efficiency point gives effective detector F aluminum layers of  $31 \mu\text{g}/\text{cm}^2$  and  $49 \mu\text{g}/\text{cm}^2$  for IMP 7 and 8 respectively. The quieter detector and thinner aluminum layer on IMP 7 gives a 50% proton detection threshold of 24 keV.

Detector G efficiencies and proton pile-up curves are shown in Figures 12 and 13.

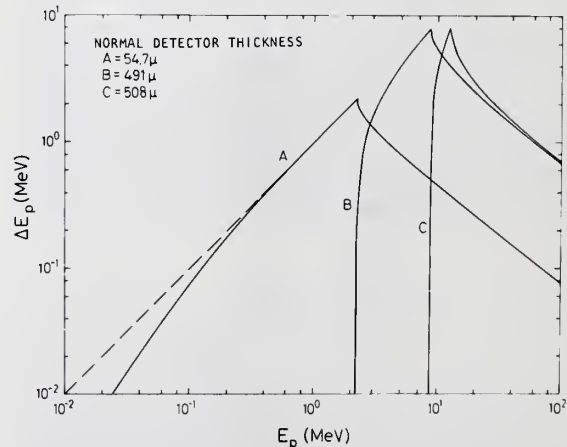


Figure 9.  $\Delta E_p$  versus  $E_p$  for the IMP 8 ABC telescope. Dashed line for detector A shows ideal curve (no absorbers), and solid line shows actual case including the measured  $60 \mu\text{g}/\text{cm}^2$  aluminum layer.

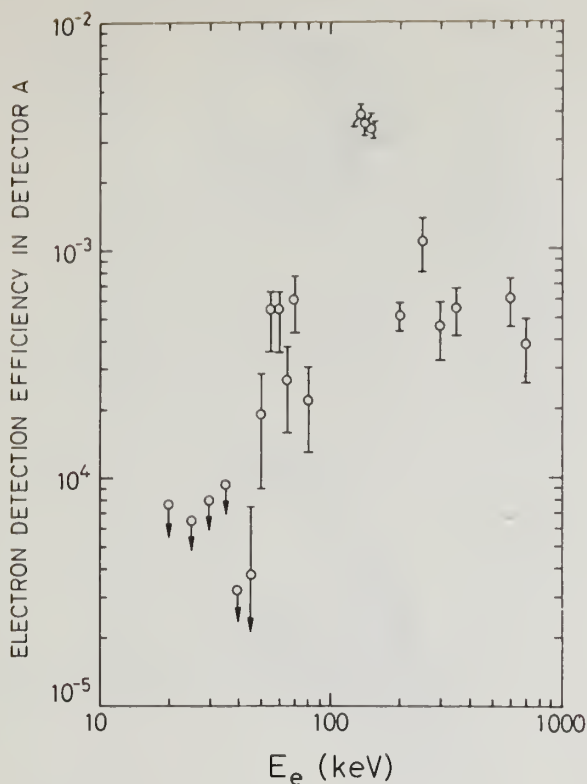


Figure 10. Main magnet assembly absolute electron detection efficiency in detector A (protons) as a function of electron energy.

Detailed electron efficiency measurements were made for detectors D and E, both in a plane perpendicular to the magnet pole faces and in a median plane between and parallel to the pole faces. From the magnet orientation in the satellite, these planes are labeled respectively the ecliptic plane and the plane perpendicular to the ecliptic plane. Absolute efficiency contours are shown in both planes for the DD<sub>2</sub> and EE<sub>2</sub> logic for IMP 8 in Figures 14 and 15. While the indicated efficiencies are reasonable for near-Earth electron detection, it is obvious that the magnet was used mainly for sweeping rather for focusing. Our present units for the ISEE A and B satellites employ focusing techniques and have a greatly extended energy range.

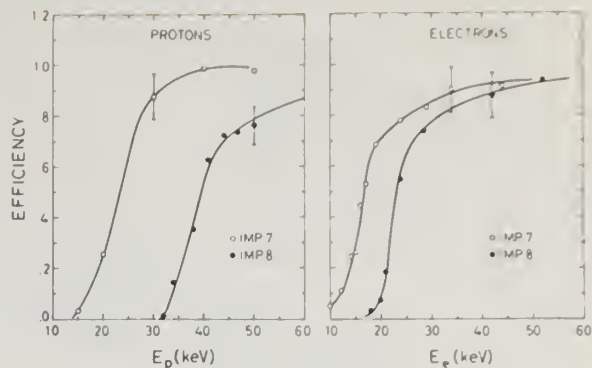


Figure 11. Low energy detector F absolute proton and electron detection efficiencies. F level = 16 keV, IMP 7; 23 keV, IMP 8.

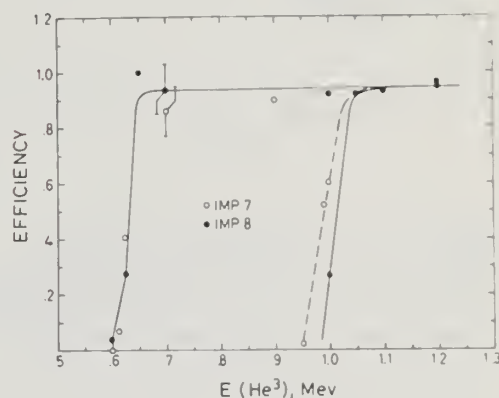


Figure 12. Absolute detection efficiencies for detector G levels G<sub>1</sub> and G<sub>2</sub>. Runs performed with He<sup>3</sup> beam.

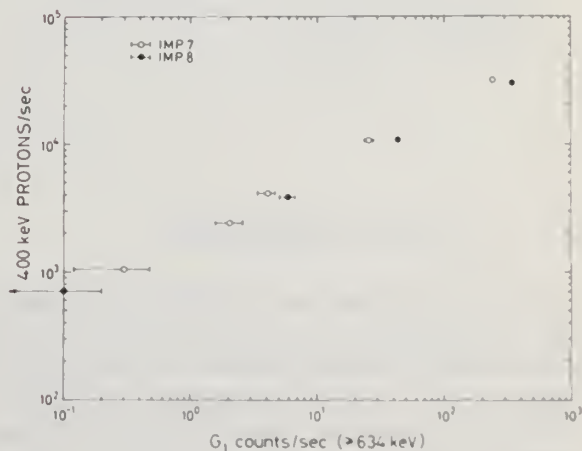


Figure 13. Measure of detector G proton contamination due to proton pile-up effects.

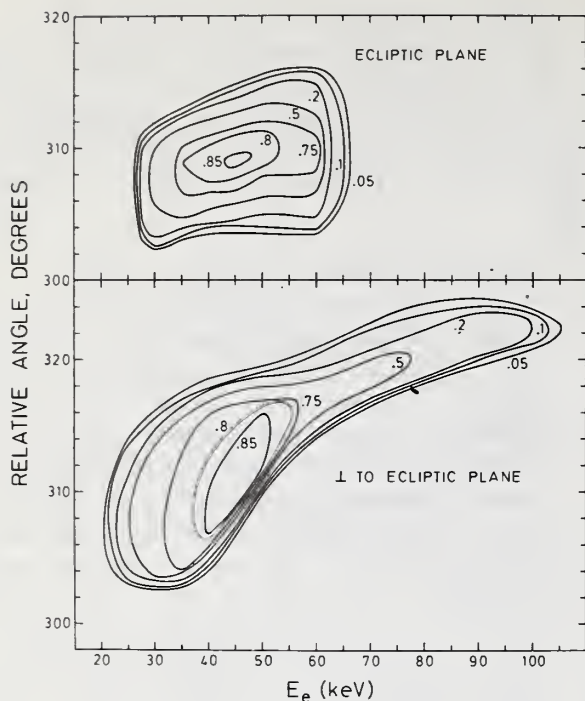


Figure 14. Absolute electron detection efficiencies for the detector D,  $D_1 D_2$  output channel. Contours of constant absolute efficiency are given in two angle-energy projections. The ecliptic plane projection is in a plane perpendicular to the magnetic pole faces. The perpendicular to ecliptic plane projection is in a plane centered between and parallel to the pole faces.

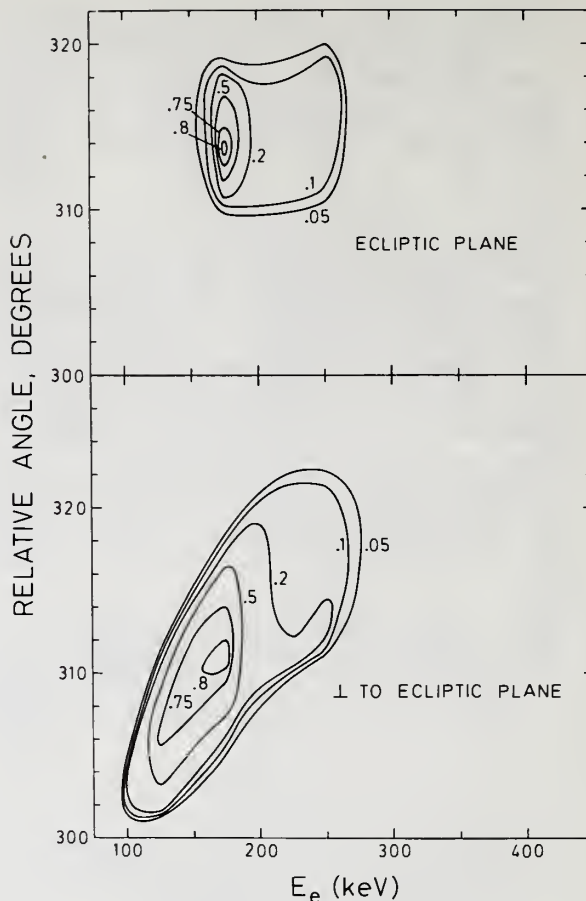


Figure 15. Absolute electron detection efficiencies for the detector E,  $E_1 E_2$  output.

## 5. IN-FLIGHT PERFORMANCE

As stated earlier, both IMP 7 and 8 EPE's have operated as expected and without malfunction since launch. Figures 16 and 17 present EPE house-keeping and calibration data from selected channels of the IMP 7 and 8 instruments. All channels display the same type of normal behavior as shown in Figures 16 and 17.

As described earlier, no problems or data losses were observed in the low energy proton channels (detector A) due to the occurrence of a sun pulse once each spin. However, the low energy threshold (30 keV) and lack of a protective foil does make the L1 channel (50-220 keV protons) sensitive to solar X-rays. This

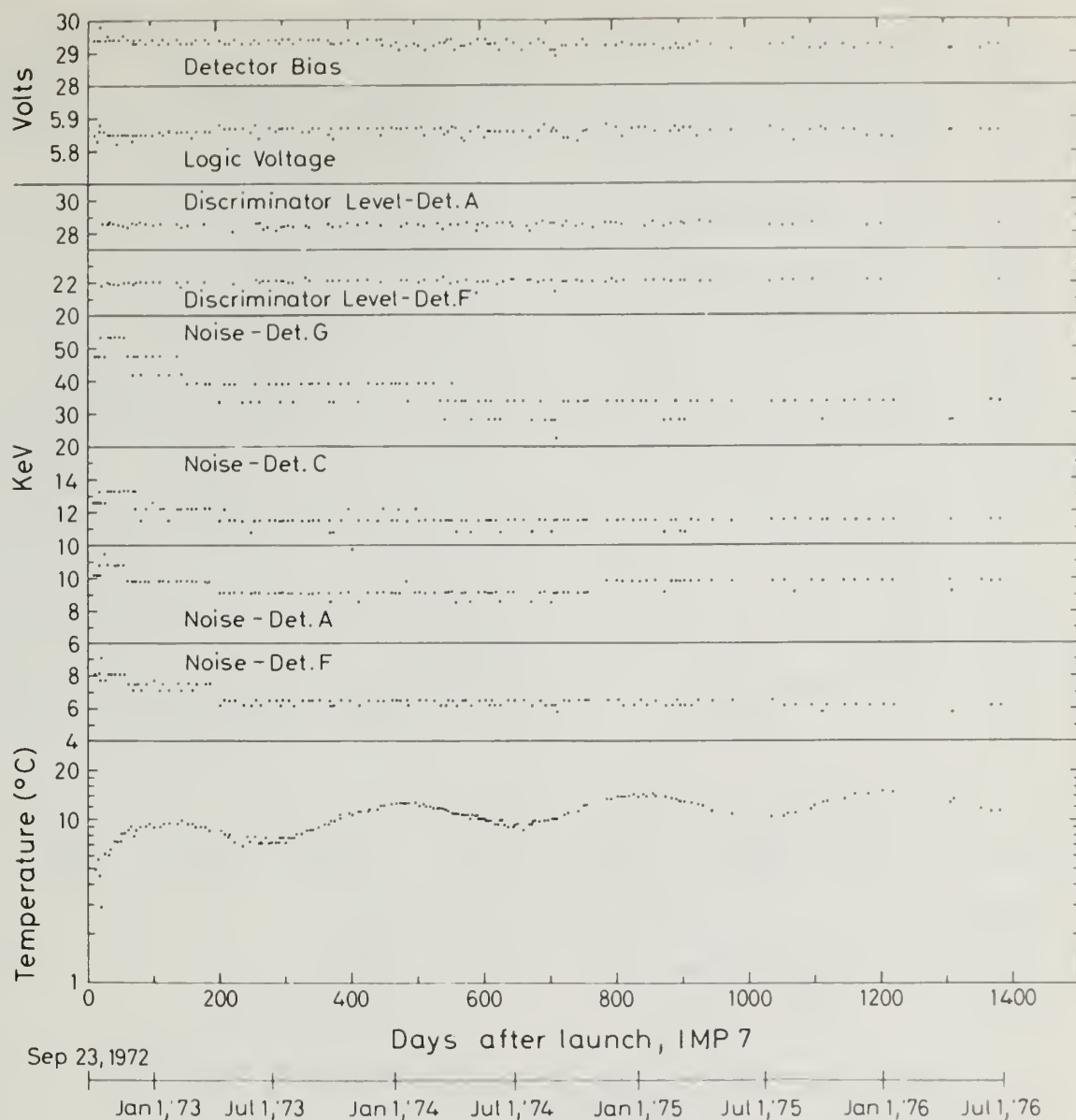


Figure 16. Several-year in-flight operational history of the IMP 7 EPE.

sensitivity has been measured in orbit using simultaneous data from IMP 7, IMP 8, and X-ray sensors on board the NOAA geostationary weather satellites, the SMS/GOES series (Unzicker and Donnelly, 1974; Grubb, 1975). A scatter plot of X-ray events observed by both SMS/GOES and

the IMP 7 EPE is shown in Figure 18 (H. Sauer, personal communication) for both the soft (0.5-2 Å) and hard (2-8 Å) X-ray components. The higher sensitivity to the hard component is clear. The normal quiet time background rate for channel L1 is ~0.1-0.2 counts per sector. IMP 8 data show nearly identical results.

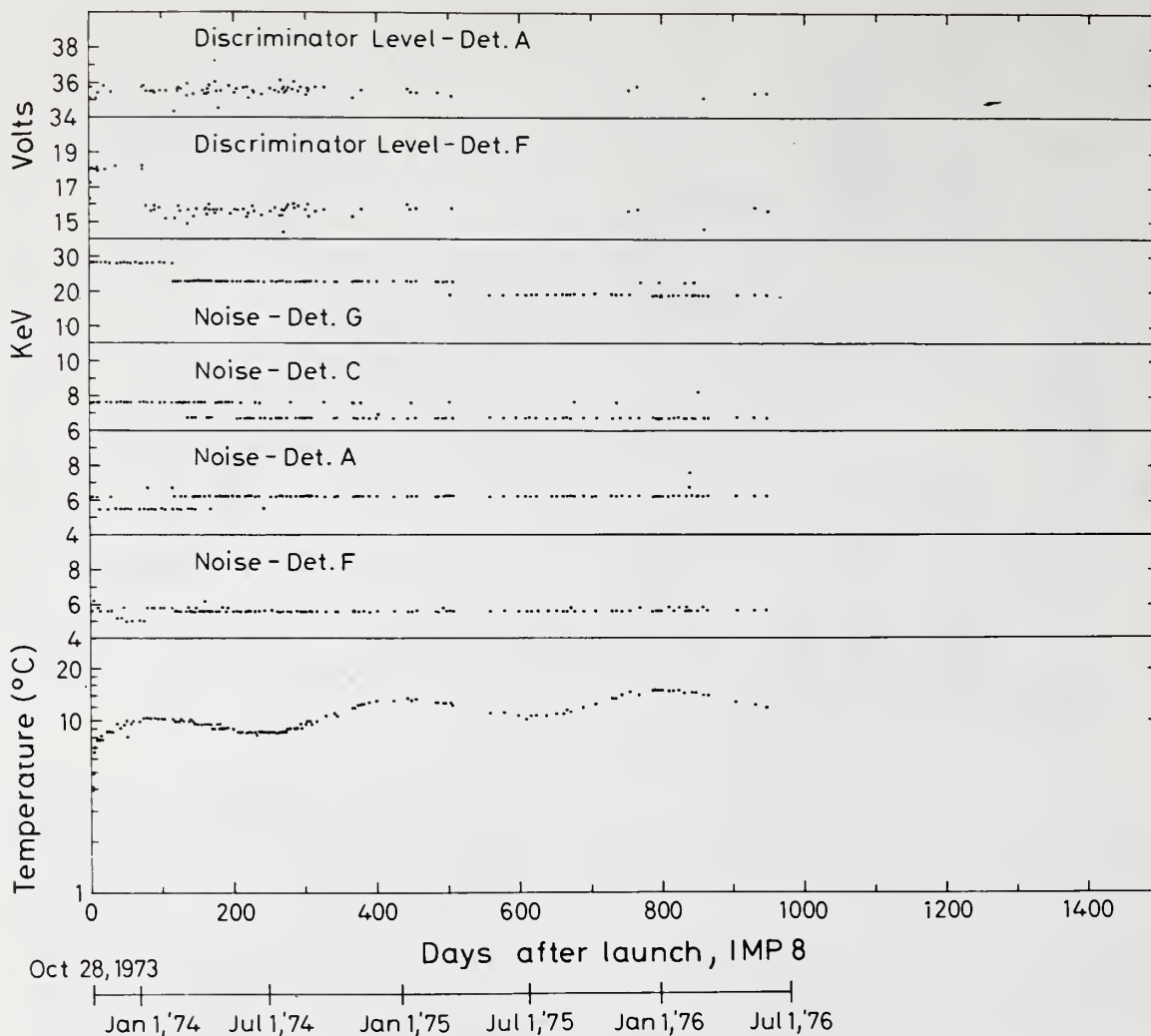


Figure 17. Several-year in-flight operational history of the IMP 8 EPE.

The X-ray sensitivity shown in Figure 18 poses no severe problems. The EPE response is confined to the solar sectors (9 and 10), is easily identified, and is not confused with proton data. In fact, the observance of an X-ray event often gives a useful timing mark for the arrival of solar particles.

## 6. GROUND DATA HANDLING

A unified EPE data set is stored on archive tapes produced from the reduction and merging of data and orbit tapes supplied by Goddard Space Flight Center. A variety of output and display programs is available for use with the archive tape.

All data are routinely processed through a program computing and displaying 30-minute count rate (counts per second) averages. A sample of the display is given in Figure 19. The data show all EPE channels from IMP 8 during the four days 19 September through 22 September 1974. A solar particle event can be seen in this interval. Vertical logarithmic scales for each channel are indicated on the left with the beginning power of ten shown for each channel at the bottom of the plot. Each plot is labeled by the appropriate channel at the first plotted point in the panel. A linear percentage bad data scale is shown at the top of the panel. For the time period of the plot, the orbit projection into the solar ecliptic plane is shown at the bottom of the panel along with a reference magnetosphere and bow shock (Fairfield, 1971).

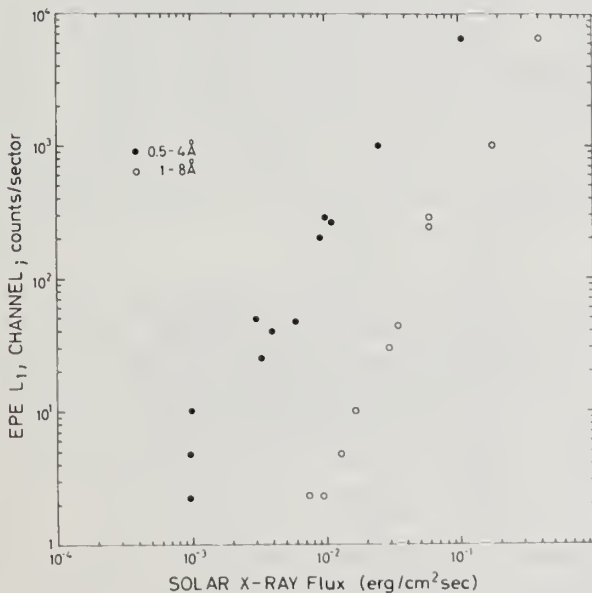


Figure 18. Plot showing measured in-flight response of EPE L1 channel (50-220 keV protons) to solar X-ray flux. Simultaneous data obtained from IMP 7 EPE and X-ray monitor on board the NOAA geostationary weather satellites (GOES). IMP 8 EPE L1 data show nearly identical response.

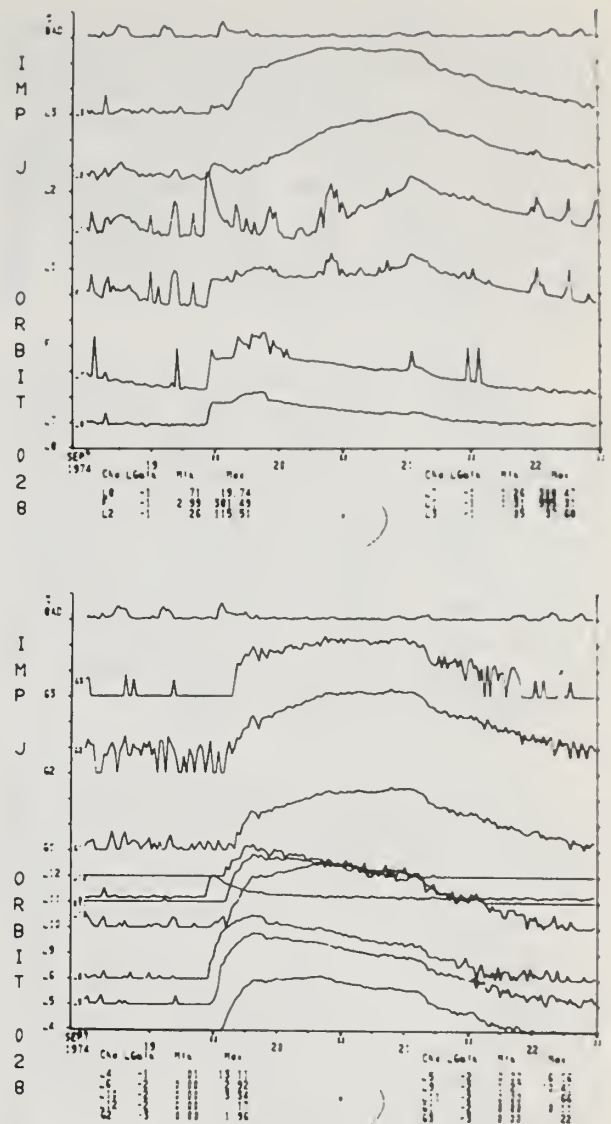


Figure 19. Standard display of 30-minute count rate averages for all EPE data channels. Logarithmic scale channel identification shown on vertical axis with each curve identified by channel indication at first point of plot. The power of ten starting each channel's logarithmic count rate scale is shown at the bottom of the panel along with maximum and minimum values recorded during the 4-day period of the plot. The satellite trajectory for that period and a reference magnetopause and bow shock are shown in the ecliptic plane.

In addition all the data from channels L1(50 keV  $\leq E_p \leq 220$  keV) and L7(30 keV  $\leq E_e \leq 100$  keV) are routinely displayed in highest time resolution for all 16 samples per spin. These displays are called poor man's plots because they are an inexpensive approximation of gray coding. A sample of our poor-man's plots is shown in Figure 20.

This display simulates gray code by printing the numerical values of the counts per sector (1/16 of a spin period) for all 16 sectors per spin. Each frame contains 20 minutes of data. The heading contains the date and hour of the current poor man's plot frame, satellite identification, and the current solar ecliptic and solar magnetospheric coordinates of the satellite in Earth radii.

The data are listed in columns. The first column gives the time in minutes and seconds of the data contained in each particular row. Columns labeled 1 through 16 contain the counts per sector for each of the 16 sectors of channel L1(52-220 keV protons) and represent one satellite spin. The column labeled L1 gives ten times the average L1 counts per sector for all 16 sectors.

The column labeled L7 gives ten times the average of selected L7 sectors (~30-100 keV electrons). Certain L7 sectors are deleted because of the reflected sunlight problem discussed earlier. The next eight columns contain 2-sector averages for channel L7. Column "7/8" contains electron spectral information. Columns F and G1 contain ten times the spin average of channels F( $E_e \geq 23$  keV,  $E_p \geq 34$  keV and G1( $E_\alpha \geq 634$  keV). The last column, labeled G, contains 10 times the proton spectral index  $\gamma$  obtained from L1 and L2, assuming a spectral form  $E^{-\gamma}$ .

Figure 20 clearly shows proton bursts observed outside the dusk magnetosphere. However, such low energy proton angular and energy distributions are significantly distorted by solar wind convection effects (50 keV protons have a velocity  $\leq 7$  times the solar wind velocity) and by the interplanetary motional electric field,  $\vec{E} = -1/c \vec{V}_{SW} \times \vec{B}$ . Consequently, in order to interpret low energy proton observations such as those shown in Figure 20, transforms into various physically meaningful coordinate frames have to be performed (Gold et al., 1975). These programs require solar wind velocity and/or interplanetary magnetic field data.

A sample of the output of such transformation programs is given in Figure 21. Polar plots of the 50-220 keV proton intensities observed by the IMP H EPE on October 31, 1972, are shown in various coordinate frames. Important directions and principal axes are shown at the top of the figure;  $\vec{V}_{SW}$  = solar wind velocity vector,  $\vec{B}$  = interplanetary magnetic field, and  $\hat{B}$  = unit vector in direction of  $\vec{B}$ .

Panel (a) of Figure 21 shows a 6-minute intensity average centered at 2034:15 hours and obtained during an intense burst of particles streaming from the magnetosphere. Solar and dotted lines give respectively the intensities observed in the satellite frame of reference and those transformed into the solar wind frame using the measured solar wind velocity of 728 km/sec (Gold et al., 1975).

Panel (b) shows a high time resolution snapshot of 20.4 seconds at 2033.34 hours and within the panel (a) 6-minute average. The solid line shows the distribution observed in the satellite frame of reference.

1/14/75	(014)	HOUR=15	IMPJ	XSE=	.3	YSE=	32.7	ZSE=	-10.6	XSM=.3	YSM=	33.6	ZSM=	-7.3															
1	2	3	4	5	6	7	8	9	10	11	12	13	14	15	16	L1	L7	1	2	3	4	5	6	7	8	7/8	F	G1	G

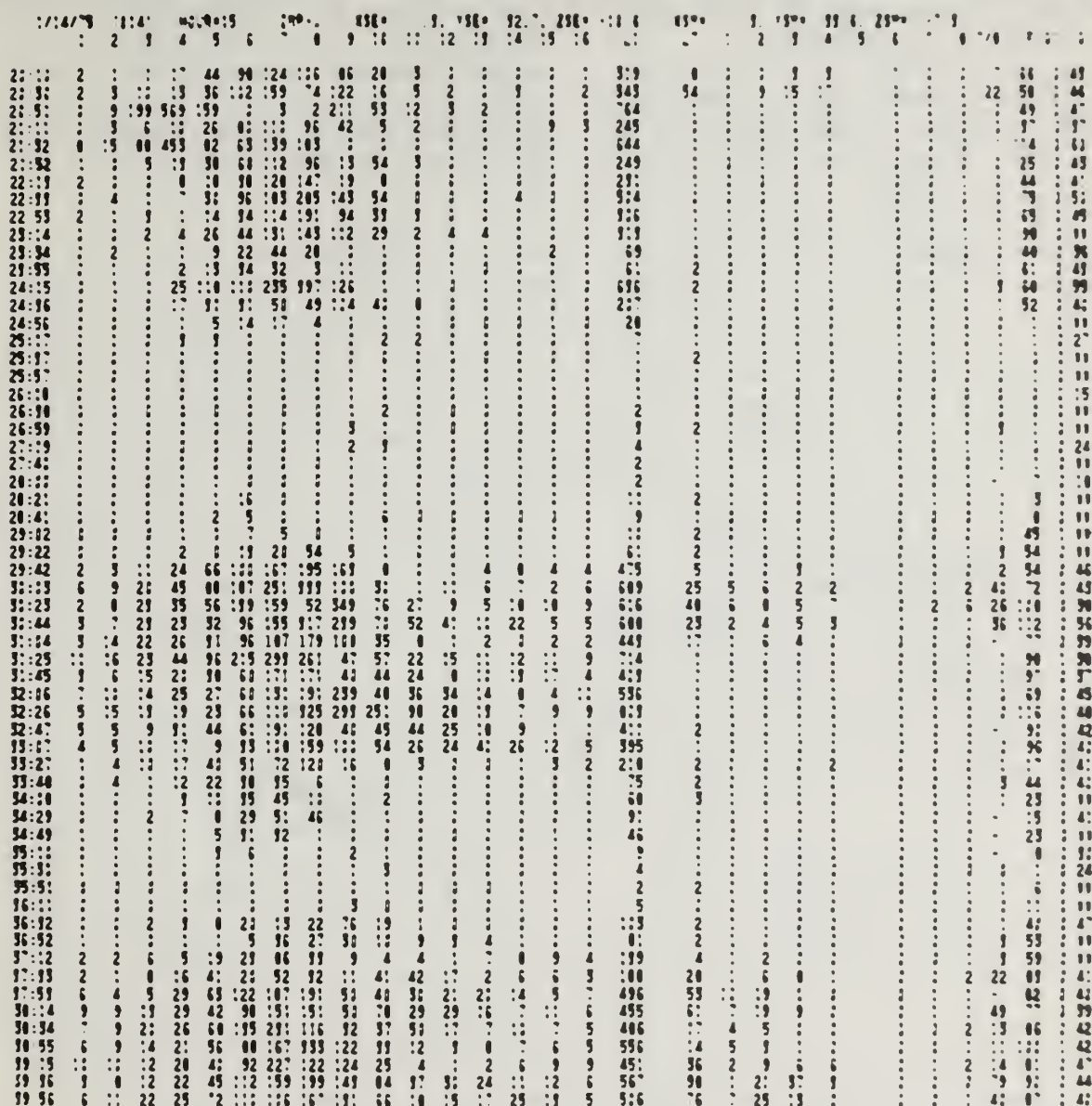


Figure 20. Poor-man's plots. Highest time resolution print-out for all sectors of L1 and L7. Time runs vertically downward, and sectors (angle in the ecliptic plane) run from left to right. This form of print-out is an inexpensive approximation of gray code. Proton bursts and their angular distribution in the satellite frame of reference are clearly visible in the display. All L1 and L7 data are available in this format.

However, in panel (b) the dotted line shows the distribution transformed according to the electric field drift velocity  $\vec{V}_E = \vec{V}_{sw} - \hat{B}\hat{B} \cdot \vec{V}_{sw}$ .

Finally panel (c) shows the particles' pitch angle distribution. Note that panel (c) shows large

intensities of ~50 keV protons filling the hemisphere along the field line viewing the magnetosphere. Also note that strong azimuthal pitch angle gradients are observed, implying the presence of strong spatial gradients having scale lengths of a 50 keV proton gyroradius ( $\approx 2.50 (10)^3$  km).

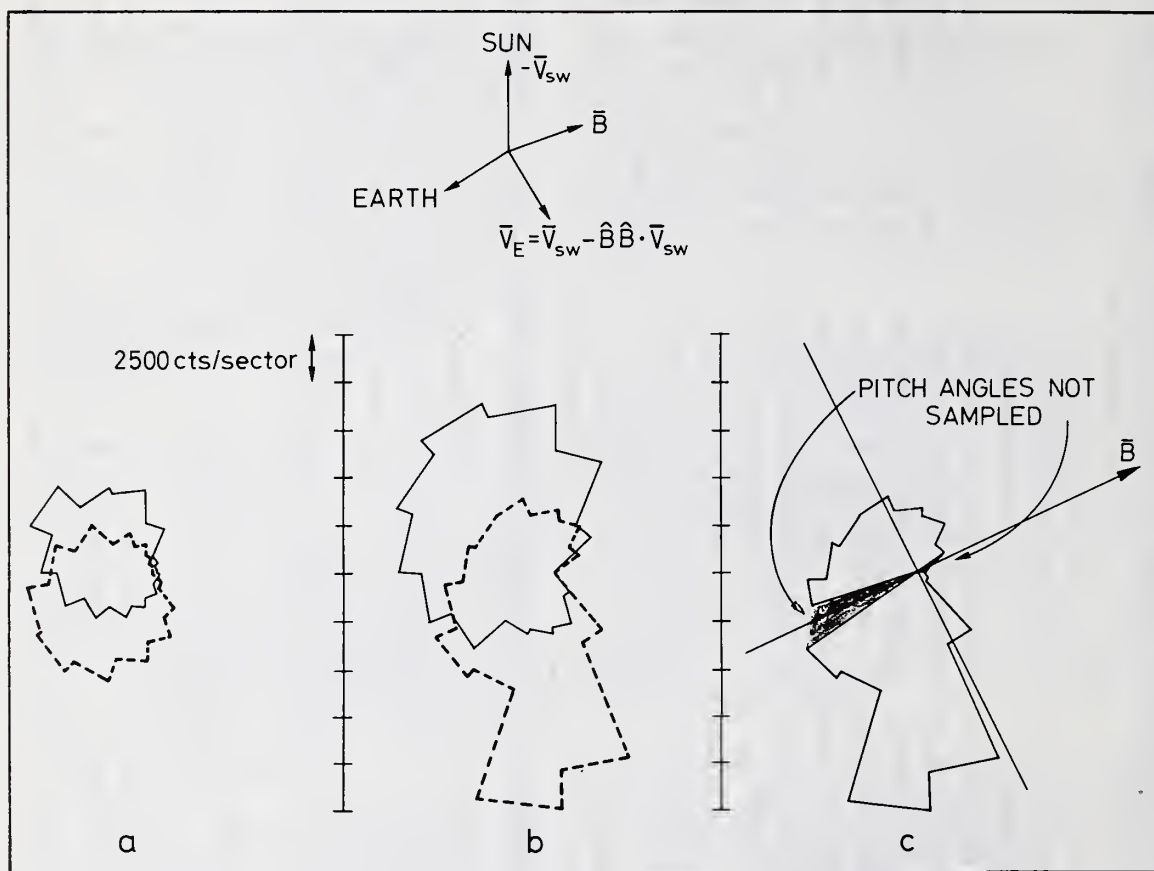


Figure 21. Polar plots of 50-220 keV proton intensities in several frames of reference. Various directions of interest are shown at the top of the figure. Panel (a): 6-min averages obtained at 2034:15 hours, 31 October 1976. The solid line shows the observations in the IMP 7 frame of reference. The dotted line shows the transformed distribution in the solar wind frame of reference using the simultaneously measured solar wind velocity of 728 km/sec. Panel (b): A 20-sec snapshot within the panel-(a) 6-min average at 2033:34 hours. The solid line again is in the satellite frame. The dotted line is in the moving frame defined by the interplanetary motional electric field drift velocity vector  $\vec{V}_E = \vec{V}_{sw} - \hat{B}\hat{B} \cdot \vec{V}_{sw}$ . Panel (c): Pitch angle distribution of panel-(b) observations.

Figure 21 clearly shows the inherent difficulty of interpreting low energy (tens to hundreds of keV) ion fluxes observed in interplanetary space in a satellite frame of reference. Data reduction must include appropriate transformations to coordinate systems of physical interest.

The low ion energies (50 keV protons) and relatively large geometric factor ( $\sim 10^{-2} \text{cm}^2 \text{ster}$ ) attained by the EPE have made it possible to estimate thermal plasma flow velocities and temperatures. Assuming a flowing Maxwellian plasma, EPE absolute proton fluxes and angular distributions have been used to obtain plasma flow velocities and temperatures in the geomagnetic tail with a sensitivity down to  $\sim 50 \text{ km/sec}$  and  $\sim 1 \text{ keV}$  for densities  $> 10^{-1} \text{cm}^{-3}$  (Roelof et al., 1976; Keath et al., 1976).

Additional reduction, analysis, and display programs exist to allow easy access to and handling of the EPE data. A detailed description of them is not appropriate here. However, they consist primarily of averaging programs, gray and color code programs, and display programs. Such a heavy investment in data handling is mandatory since the productivity of large experimental data sets is proportional to their accessibility.

## 7. ACKNOWLEDGMENTS

The EPE project was a collaborative effort between the National Oceanic and Atmospheric Administration Space Environment Laboratory and the Johns Hopkins University Applied Physics Laboratory, and it is not possible to acknowledge all the people who contributed to its success. However, I do wish to acknowledge those who had major responsibilities and those whose efforts got the

EPE successfully through several difficult situations. The following individuals provided invaluable and major contributions in the areas indicated; C. O. Bostrom, Co-investigator, all phases of the experiment; J. R. Cessna and T. A. Fritz, detectors, detector head assembly and calibration; A. F. Hogrefe, R. Cashion, S. A. Gary, and D. P. Peletier, electronics, EPE assembly and test, spacecraft integration; G. Glaeser, mechanical design; J. Crawford, detector qualification; R. Thomson, fabrication; J. W. Kohl, calibration; S. Brown and The Goddard Space Flight Center calibration facility; the Naval Research Laboratory accelerator staff; M. Gallucci, data reduction and display system; W. Burkey, data and housekeeping logs. Finally I wish to acknowledge the efforts of the Goddard Space Flight Center IMP project office in making the IMP 7 and 8 programs so successful. Their mixture of professionalism, pragmatism, and wit made this not only a successful mission but also an enjoyable one.

I wish to acknowledge and thank A. Lazarus and R. Lepping for making readily available the solar wind velocity and magnetic field data that are required for the transforms shown in Figure 21.

## 8. REFERENCES

- Coleman, J. P., D. P. Love, J. H. Trainor, and D. J. Williams (1968a): Low energy proton damage effects in silicon surface barrier detectors. IEEE Trans. Nucl. Sci., NS-15(1), 482.
- Coleman, J. P., D. P. Love, J. H. Trainor, and D. J. Williams (1968b): Effects of damage by 0.8 MeV-5.0 MeV protons in silicon surface barrier detectors. IEEE Trans. Nucl. Sci., NS-15(3), 363.

- Elad, E., C. M. Inskeep, R. A. Sareen, and P. Nestor (1973): Dead layers in charged particle detectors. IEEE Trans. Nucl. Sci., NS-20(1), 534.
- Fairfield, D. H. (1971): Average and unusual locations of the earth's magnetopause and bow shock. J. Geophys. Res., 76, 6800.
- Fritz, T. A., and J. R. Cessna (1975): ATS-6 NOAA low energy proton experiment. IEEE Trans. on Aerosp. and Electronics Systems, AES-11(6), 1145.
- Gary, S. A. (1970): EPE preamplifiers/channels F and G. Applied Physics Laboratory Internal Report S1P-591-70.
- Gold, R. E., C. O. Bostrom, E. C. Roelof, and D. J. Williams (1975): Anisotropy of ~50 keV solar protons in the spacecraft and co-moving frames. Proc. Int. Conf. Cosmic Rays 14th, 5, 1801.
- Grubb, R. N. (1975): The SMS/GOES space environment monitor subsystem. NOAA Technical Memorandum ERL SEL-42.
- Hogrefe, A. F. (1970): Preamplifiers for the energetic particle experiment IMP H and J. Applied Physics Laboratory Internal Report S1P-615-70.
- Inskeep, C., E. Elad, and R. A. Sareen (1974): Surface barrier structures with various metal electrodes. IEEE Trans. Nucl. Sci., NS-21(1), 1.
- Keath, E. P., E. C. Roelof, C. O. Bostrom, and D. J. Williams (1976): Fluxes of >50 keV protons and >30 keV electrons at 35 R<sub>e</sub> morphology and flow patterns in the magnetotail. J. Geophys. Res., 81, 2315.
- Keppler, E., B. Wilken, K. Richter, G. Umlauf, K. Fischer, and H. P. Winterhoff (1976): Ein spektrometer für geladene teilchen mittlerer energien-experiment E8, HELIOS. Bundesministerium für Forschung und Technologie, Forschungs-bericht BMFT-FBW 76-14, Max-Planck-Institut für Aeronomie.
- Longanecker, G. W. and R. A. Hoffman (1973): S<sup>3</sup>-A spacecraft and experiment description. J. Geophys. Res., 78, 4711.
- Peletier, D. P. (1970): IMP H and J EPE in-flight calibrator. Applied Physics Laboratory Internal Report S1P-614-70.
- Roelof, E. C., E. P. Keath, C. O. Bostrom, and D. J. Williams (1976): Fluxes of >50 keV protons and >30 keV electrons at 35 R<sub>e</sub> velocity anisotropy and plasma flow in the magnetotail. J. Geophys. Res., 81, 2304.
- Unzicker, A., and R. F. Donnelly (1974): Calibration of X-ray ion chambers for the space environment monitoring system. NOAA Technical Report ERL 310-SEL 31.
- Wilken, B., and T. A. Fritz (1974): The response of very thin semiconductor detectors to heaving ions: I. Protons and helium. Nucl. Inst. and Methods, 121, 365.
- Wilken, B., and T. A. Fritz (1976): Energy distribution functions of low energy ions in silicon absorbers measured for large relative energy losses. Nucl. Inst. and Methods, 138, 331.
- Williams, D. J., R. A. Hoffman, and G. W. Longanecker (1969): The small scientific satellite (S<sup>3</sup>) program and its first payload. IEEE Trans. Nucl. Sci., NS-16(1), 322.





# Environmental Research LABORATORIES

The mission of the Environmental Research Laboratories (ERL) is to conduct an integrated program of fundamental research, related technology development, and services to improve understanding and prediction of the geophysical environment comprising the oceans and inland waters, the lower and upper atmosphere, the space environment, and the Earth. The following participate in the ERL missions.

<b>MESA</b>	<i>Marine EcoSystem Analysis Program</i> . Plans, directs, and coordinates the regional projects of NOAA and other federal agencies to assess the effect of ocean dumping, municipal and industrial waste discharge, deep-sea mining, and similar activities on marine ecosystems.	<b>GFDL</b>	<i>Geophysical Fluid Dynamics Laboratory</i> . Studies the dynamics of geophysical fluid systems (the atmosphere, the hydrosphere, and the cryosphere) through theoretical, analytical, and numerical simulation using powerful high-speed digital computers.
<b>OCSEA</b>	<i>Outer Continental Shelf Environmental Assessment Program Office</i> . Plans and directs research studies supporting the assessment of the primary environmental impact of energy development along the outer continental shelf of Alaska; coordinates related research activities of federal, state, and private institutions.	<b>APCL</b>	<i>Atmospheric Physics and Chemistry Laboratory</i> . Studies drag and precipitation, photochemical, and particulate composition of the atmosphere, atmospheric electricity, and atmospheric heat transfer, with emphasis on developing methods of beneficial weather modification.
<b>WM</b>	<i>Weather Modification Program Office</i> . Plans, directs, and coordinates research within ERL relating to precipitation enhancement and mitigation of severe storms. Its National Hurricane and Experimental Meteorology Laboratory (NHEML) studies hurricane and tropical cumulus systems to experiment with methods for their beneficial modification and to develop techniques for better forecasting of tropical weather. The Research Facilities Center (RFC) maintains and operates aircraft and aircraft instrumentation for research programs of ERL and other government agencies.	<b>NSSL</b>	<i>National Severe Storms Laboratory</i> . Studies severe storm circulation and dynamics, and develops techniques for threat and hazard forecasting, thunderstorms, and severe cold.
<b>AOML</b>	<i>Atlantic Oceanographic and Meteorological Laboratories</i> . Studies the physical, chemical, and geological characteristics and processes of the ocean waters, the sea floor, and the atmosphere above the ocean.	<b>WPL</b>	<i>Wave Propagation Laboratory</i> . Studies the propagation of sound waves and electromagnetic waves at megahertz, infrared, and optical frequencies to develop new methods for remote measuring of the geophysical environment.
<b>PMEL</b>	<i>Pacific Marine Environmental Laboratory</i> . Monitors and predicts the physical and biological effects of man's activities on Pacific Coast estuarine, coastal deep-sea, and near-shore marine environments.	<b>ARL</b>	<i>Air Resources Laboratory</i> . Studies the diffusion, transport, and deposition of atmospheric pollutants; develops methods of predicting and monitoring atmospheric pollution; monitors the atmospheric environment to detect climatic change.
<b>GLERL</b>	<i>Great Lakes Environmental Research Laboratory</i> . Studies hydrology, waves, currents, lake levels, biological and chemical processes, and lake-air interaction in the Great Lakes and their watersheds; forecasts lake ice conditions.	<b>AL</b>	<i>Aeronomy Laboratory</i> . Studies the physical and chemical processes of the atmosphere, ionosphere, and exosphere of the Earth and other planets, and their effect on both annual meteorological phenomena.
		<b>SEL</b>	<i>Space Environment Laboratory</i> . Studies solar-terrestrial physics (interplanetary, magnetospheric, and ionospheric), develops techniques for forecasting solar disturbances, provides real-time monitoring and forecasting of the space environment.

**U.S. DEPARTMENT OF COMMERCE**  
National Oceanic and Atmospheric Administration  
BOULDER, COLORADO 80302

PENN STATE UNIVERSITY LIBRARIES



A000072021897